

RETRIEVAL OF AGROMETEOROLOGICAL PARAMETERS USING SATELLITE REMOTE SENSING DATA

S. K. Saha

Agriculture and Soils Division

Indian Institute of Remote Sensing, Dehra Dun

Abstract : The recent development of satellite meteorology has allowed us to estimate spatially and frequently number of basic agro-meteorological parameters. This paper discusses approaches of retrieval of several agro-meteorological parameters viz. surface albedo, land surface temperature, evapotranspiration, absorbed photosynthetically active radiation by integrated use of optical and thermal infrared sensors satellite data.

INTRODUCTION

Countries in the Asia-Pacific region have networks of agro-meteorological ground stations in order to monitor the agricultural production and weather forecasting. But, such networks are generally less dense than they should be for a correct representation of the high spatial climatic variability which exists in Asia-Pacific region. Also the agro-meteorological data from various ground stations are not delivered in real time to a central collecting point. So, conventional agro-meteorological techniques have severe limitations to use their data for real time agricultural monitoring and yield forecasting.

The recent development of satellite meteorology has allowed us to obtain frequent and accurate measurements of a number of basic agro-meteorological parameters (e.g. surface albedo, surface temperature, evapotranspiration, solar radiation, rainfall etc.). The satellite estimated agro-meteorological parameters have several advantages compared to conventional measurements of agro-meteorological data in ground meteorological network.

- The spatial scale, from 50 m to 5 km depending on the satellite resolution, is more precise than ground climatic data (typically near 100 km for synoptic stations and 10-50 km for local less regular stations).
- High temporal data (e.g. every half an hour for METEOSAT).
- Remote sensing has access to surface agromet properties, as opposed to screen height agromet data in conventional method which attempts to characterize air mass properties.

The various approaches of retrieval of several agro-meteorological parameters viz. Surface albedo, Surface temperature, Evapotranspiration (ET), Absorbed photo-synthetically active radiation (APAR) using satellite data are discussed in following sections.

APPROACHES OF RETRIEVAL OF AGRO-METEOROLOGICAL PARAMETERS USING SATELLITE DATA

Surface Albedo

The amount of solar radiation (0.4 – 4.0 μm) reflected by a surface is characterized by its hemispherical albedo, which may be defined as the reflected radiative flux per unit incident flux. Surface albedo is an important parameter used in global climatic models to specify the amount of solar radiation absorbed at the surface. Moreover, variations in surface albedo can serve as diagnostic of land surface changes and their impact on the physical climatic system can be assessed when routinely monitored surface albedo is used in climatic models. Albedo information is useful for monitoring crop growth, prediction of crop yield, and monitoring desertification.

For clear sky conditions, the surface albedo may be estimated by remote sensing measurements covering optical spectral bands.

The albedo 'A', can generally be expressed by the following equations (Valientez *et al.*, 1995) :

$$A = (\pi \cdot L_{\lambda}) / (\mu_s \cdot E_s)$$

where L is the integral of the spectral irradiance weighted by the filter function of the band ($\text{W}/\text{m}^2/\text{Sr}$) and E_s is the integral of the spectral solar irradiance weighted by the filter function (W/m^2).

$$\mu s = \text{Cos } \theta s$$

$$\pi. L = \int_{\lambda^a}^{\lambda^b} \pi. L (\lambda). S(\lambda). d\lambda$$

$$\mu s. Es = \int_{\lambda^a}^{\lambda^b} \mu s. Es (\lambda). S(\lambda). d\lambda$$

where, $L (\lambda)$ is the spectral radiance reflected from the surface ($\text{W}/\text{m}^2/\text{Sr}/\mu\text{m}$); $S (\lambda)$ is the spectral response of the filter function; $Es (\lambda)$ is the normal spectral irradiance coming from the sun ($\text{W}/\text{m}^2/\mu\text{m}$).

Goita and Royer (1992) suggested the following equation for computation of albedo, using atmospherically uncorrected reflectance :

$$A = \frac{\sum_{i=1}^n \rho_i . E_i}{\sum_{i=1}^n E_i}$$

$$\rho = \pi . L \lambda . d^2 / E_i . \text{Cos } \theta s$$

$$L \lambda = \alpha . \text{DN} + \beta$$

where, ρ_i is the apparent reflectance in band i ; E_i is the exo-atmosphere solar irradiance in band i , $L \lambda$ is the spectral radiance; d^2 is the sun to earth distance correction factor; θs is the solar zenith angle; DN is the digital number; α and β are the gain and off-set values obtained from the sensor calibration parameters.

The general term “narrow-band” include Landsat, IRS, AVHRR channels, while the general term “broad-band” include METEOSAT. The term “Planetary” and “Surface” refer to either albedo when they are calculated or measured from top of the atmosphere as seen by a satellite or at ground level without any intermediate atmosphere, respectively.

Several factors complicate the estimation of surface albedo from remotely sensed data-atmospheric effect, degree of isotropy of the surface and spectral interval of the narrow band interval (Brest and Goward, 1987).

Rugged terrain, the geometry between the sun, the surface orientation and the satellite sensor, which can vary from one pixel to another is a factor which makes the estimation of surface reflectance from remotely sensed data difficult.

Saunders (1990) suggested a detailed complex methodology to retrieve surface albedo from NOAA – AVHRR visible and infrared bands by considering Rayleigh scattering, aerosol scattering and gaseous absorption as the principal radiation attenuating mechanisms, wherein the accuracy of the atmospheric correction would be dependent on input profiles of atmospheric constituents.

Prasad *et al.* (1995) suggested a dark body radiance method for computation of albedo from NOAA – AVHRR data and found albedo values comparable to those retrieved by Saunders (1990) method. The methodology adopted by them is discussed below :

The albedo (A) is given by

$$A = W_1 \cdot \rho_1 + W_2 \cdot \rho_2$$

where, ρ_1 and ρ_2 are atmospherically corrected reflectance factors for the visible and near IR band, respectively. W_1 and W_2 are the weightages specific to spectral bands (given by Saunders, 1990). The atmospherically corrected reflectance for the pixel in a given band (ρ_1) is given by :

$$\rho_1 = (L_p - H_p) / [S \cdot \sin(r) - B_p \cdot H_p]$$

where, L_p is the radiance for pixel 'p'; $S \cdot \sin(r)$ represents the extra-terrestrial solar spectral radiation which depends on the sun elevation angle 'r' and the day of the year; H_p is the atmospheric radiance component for a given pixel 'p' at scan/view angle θ_p (from local vertical) :

$$H_p = H_n \cdot \sec \theta_p$$

$$H_n = H_B \cdot \sec \theta_B$$

$$B_p = [1 - (f)_p] / (b)_p$$

where, H_B is the base radiance of dark body pixels (water body for NIR and the cloud shadow region for visible band) due to atmospheric effects; H_n is the normalized atmospheric radiance for nadir, θ_B is the scan angle for the base pixels; $(f)_p$ and $(b)_p$ refer to forward and backward scattering for the pixel at wavelength.

Saha and Pande (1995a) used Landsat TM optical bands data for computation of regional surface albedo following the approach suggested by Goita and Royer (1992) (Fig. 1). An albedo image was generated by Kant (2000) for the snow and forest covered Himalayan mountain of India by using NOAA – AVHRR Ch1 and Ch2 data following an empirical relationship relating broad band albedo and narrow band albedo (Fig. 2).

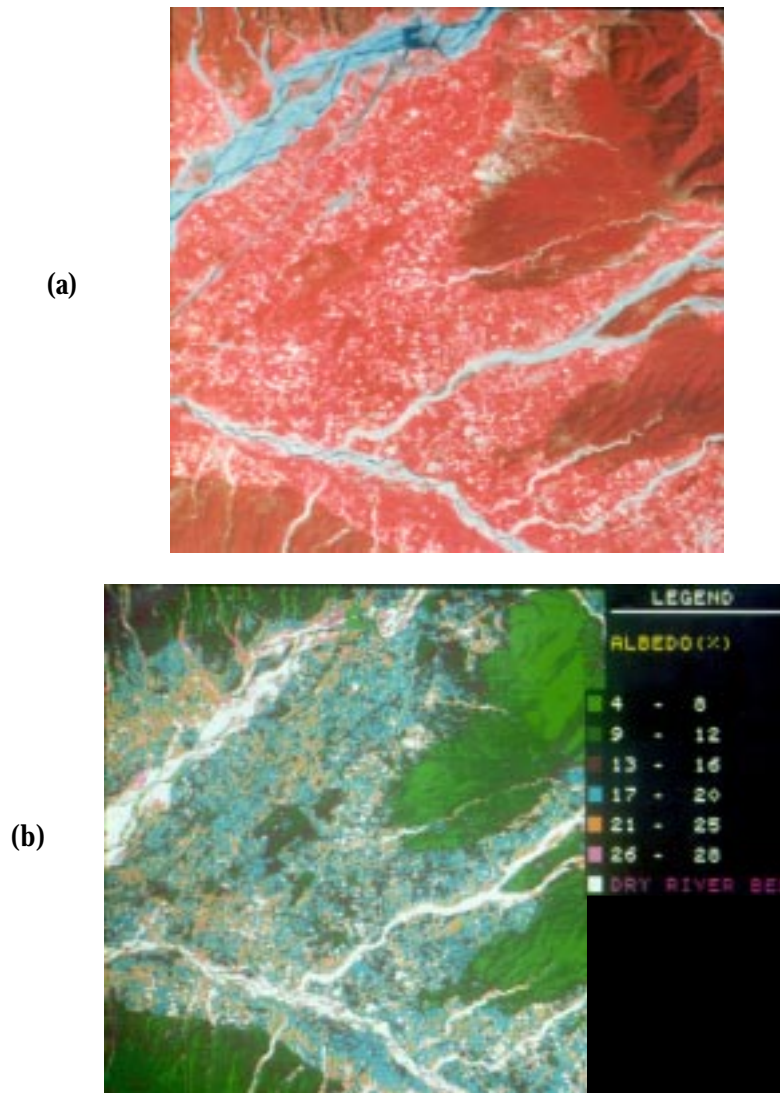


Figure 1: (a) FCC and (b) Albedo image of part of Doon Valley generated by using Landsat-TM optical data

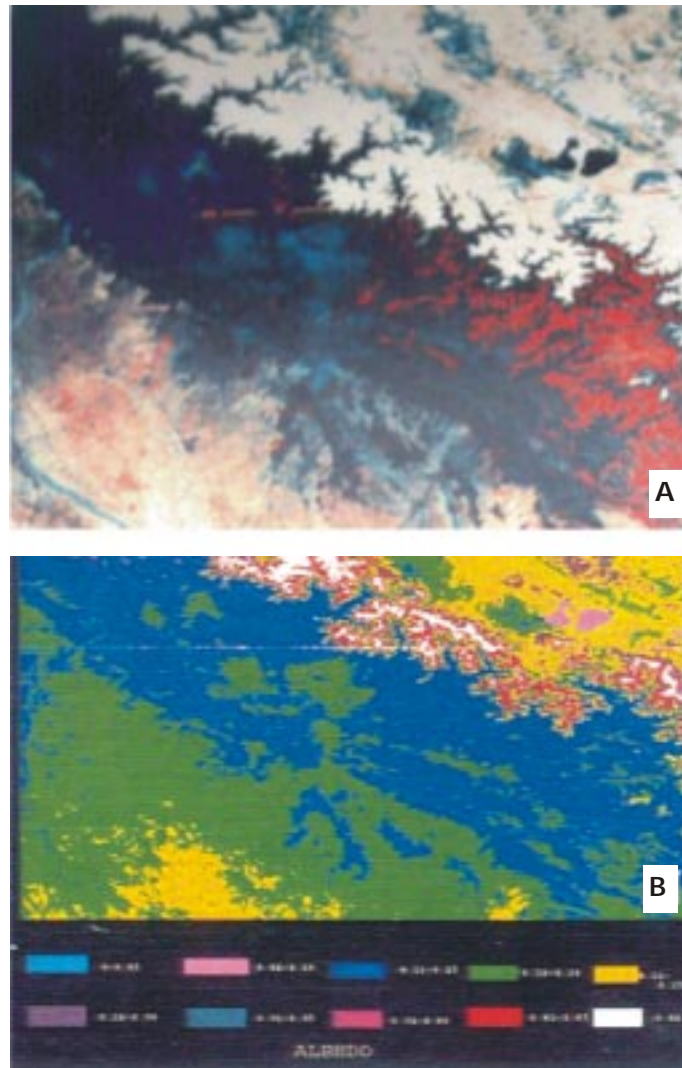


Figure 2: (A) FCC (NOAA-AVHRR-Ch2,Ch1,Ch1) and (B) Albedo image of Part of Himalayan mountain, India

Land Surface Temperature

It is the temperature of the land surface i.e. kinetic temperature of the soil plus the canopy surface (or in the absence of vegetation, the temperature of the soil surface).

Surface temperature can be used for various agro-meteorological applications –

- surface heat energy balance study
- characterization of local climate in relation with topography and land use
- mapping of low temperature for frost conditions (night-time) or winter cold episodes (day/night)
- derivation of thermal sums (using surface temperature instead of air temperature) for monitoring crop growth and development conditions.

The land surface temperature can be estimated from remote sensing measurement at thermal IR wavelength (8-14 μm) of the emitted radiant flux (L_i) and some estimate of the surface emissivity (ϵ). Land surface temperature (T_s) can be expressed using inverse Plank's equation (Mansor and Cracknell, 1994) :

$$T_s = C_2 / \lambda \ln [(\epsilon \cdot C_1 \cdot \lambda^{-5} / \pi \cdot L\lambda) + 1]$$

where, C_1 and C_2 are the first and second radiation constants ($C_1 = 3.742 \times 10^{-16} \text{ Wm}^2$ & $C_2 = 0.01444 \text{ mK}$); λ is wavelength in m; ϵ is the emissivity and $L\lambda$ is the spectral radiance ($\text{mw/cm}^2/\text{Sr}/\mu\text{m}$).

The Normalised Difference Vegetation Index (NDVI) is used as a parameter for evaluating emissivity. The surface emissivity of a surface can be calculated using the following relationship (van de Griend, 1993) :

$$\epsilon = a + b \cdot \ln(i) + \Delta\epsilon$$

where, $a = 1.0094$ and $b = 0.047$, 'i' is the NDVI of mixed pixel, $\Delta\epsilon$ is the error in emissivity values. 'i' can be estimated by using following expressions (Valor and Caselles, 1996) :

$$i = i_v \cdot P_v + i_g (1 - P_v)$$

$$P_v = (1 - i/i_g) / (1 - i_v/i_g) - K (1 - i/i_v)$$

$$K = (\rho_{2v} - \rho_{1v}) / ((\rho_{2g} - \rho_{1g}))$$

where, P_v is the vegetation proportion; 'i' is the NDVI value of mixed pixel; i_g and i_v are the NDVI values of pure soil and pure vegetation pixel, respectively,

ρ_{2v} and ρ_{1v} are the reflectances in NIR and red region for pure vegetation pixels; ρ_{2g} , ρ_{1g} are the reflectances in NIR and red region for pure soil pixels.

$$\Delta\epsilon = 4 < d\epsilon > P_v (1 - P_v)$$

where, $\Delta\epsilon$ is mean weighed value taking into account the different vegetation in the area, their structure and their proportion in it.

The NOAA – AVHRR channels 4 & 5 (10.3 – 10.3 and 11.5 – 12.5 μm) are widely used for deriving surface temperature for the day time passes. The temperatures derived from channels 4 and 5 are slightly different due to atmospheric water vapour absorption. Thus, in the land surface retrieval algorithm, the incorporation of the difference between channels 4 & 5 could be useful in correcting for the atmospheric water vapour effect as a first degree approximation. An approach based on the differential absorption in two adjacent infrared channels is called “split-window” technique and is used for determination of surface temperature.

In split-window algorithm, brightness temperatures in AVHRR channel 4 (T_4) and channel 5 (T_5), mean emissivity ϵ , i.e. $(\epsilon_4 + \epsilon_5)/2$; difference in emissivity $\Delta\epsilon$, i.e. $(\epsilon_4 - \epsilon_5)$, have been used for the estimation of land surface temperature using the following relation (Becker and Li, 1990) :

$$T_s = A + B [(T_4 + T_5) / 2] + C [(T_4 - T_5) / 2]$$

where, A, B and C are co-efficients worked out by statistical analysis and given by :

$$A = 1.274; B = 1 + \{0.15616 (1 - \epsilon) / \epsilon\} - 0.482 (\Delta\epsilon / \epsilon^2)$$

$$C = 6.26 + \{ 3.98 (1 - \epsilon) / \epsilon\} + 38.33 (\Delta\epsilon / \epsilon^2)$$

Brightness temperature (T_B) values have been calculated by using the inverse of Planck's radiation equation :

$$T(B) = C_2 \cdot V / 1_n (1 + C_1 \cdot V^3 / E_i)$$

$$E_i = S_i \cdot C + I_i \text{ (Kidwell, 1991)}$$

where, V is the wave number of (Cm^{-1}) of channel filter;

$$C_1 = 1.1910659 \times 10^{-5} \text{ (mw/m}^2\text{/Sr/cm}^4\text{)}$$

$$C_2 = 1.43883 \text{ cm}^{\circ}\text{k}$$

E_i , is radiance ($\text{mw/m}^2\text{/Sr/cm}$); C is digital number; S_i scaled slope; I_i is the intercept value.

Flow diagram of the methodology for deriving land surface temperature following “split-window” approach using NOAA – AVHRR data is shown in Fig. 3. Landsat TM (Saha and Pande, 1995a) and NOAA – AVHRR derived (Kant, 2000) land surface temperature images generated following above approaches are presented in Fig. 4 and Fig. 5, respectively.

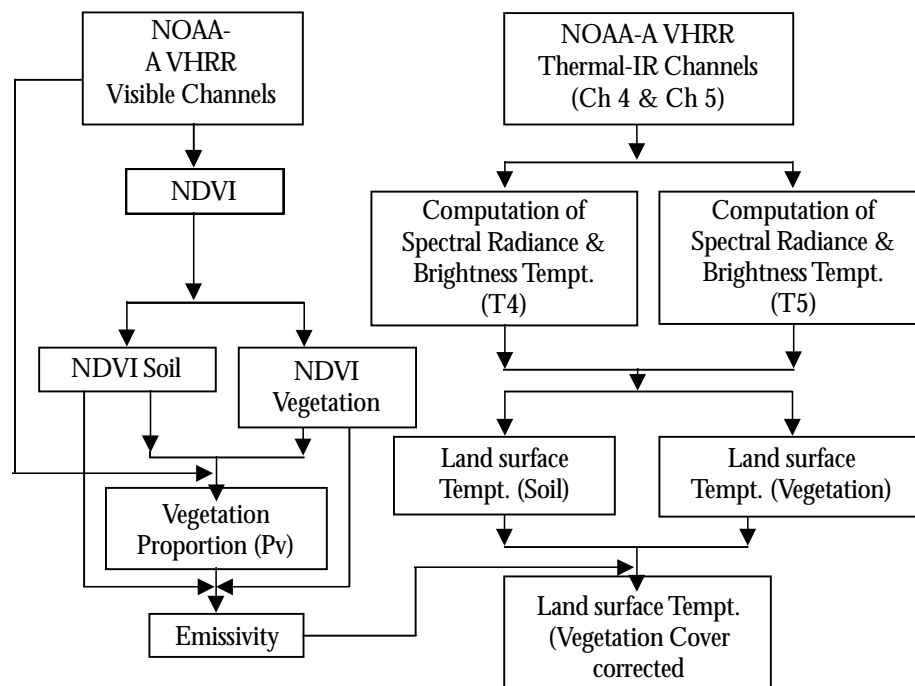


Figure 3: Flow diagram of methodology of retrieval of land surface temperature using NOAA-AVHRR data.



Figure 4: Surface temperature image generated by processing of Landsat – TM in part of western Doon Valley, Dehra Dun

Evapotranspiration (ET)

The concept of using remotely sensed surface temperature in evapotranspiration estimation has been demonstrated by Bartholic *et al.* (1972) and Brown (1974).

The model used to estimate evapotranspiration from remote sensing data and agro-meteorological data is based on surface energy balance equation.

$$R_n = G + H + LE$$

$$LE = R_n - H - G$$

where, R_n is the net radiation flux; LE is the latent heat flux (corresponding to evaporation for a bare soil and evapotranspiration for a vegetation canopy); H is the sensible heat flux; G is the soil heat flux. All above terms have unit W / m^2 . The net radiation (R_n) can be expressed as :

$$R_n = (1-A) R_s + E_a \cdot R_l - E_s \cdot \sigma \cdot T_s^4$$

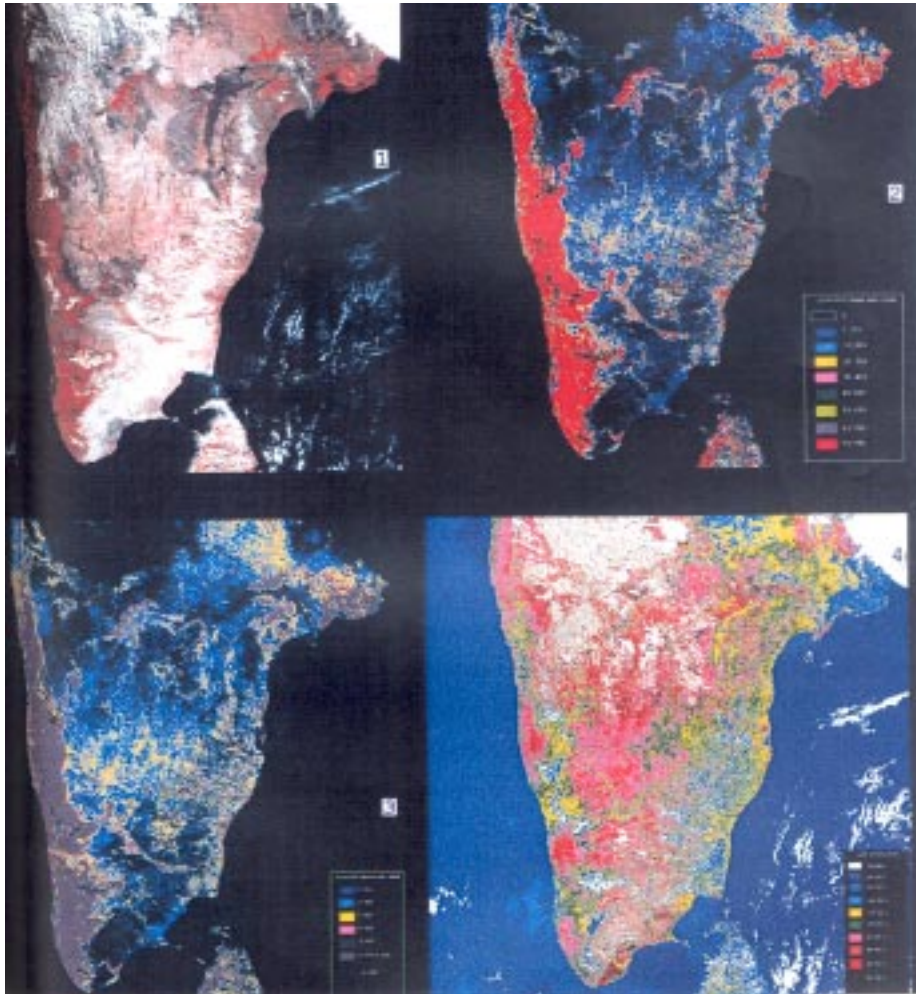


Figure 5: (1) FCC (Ch2, Ch1, Ch1, R,G,B) ; (2) Vegetation proportion image; (3) Surface emissivity image and (4) Surface Temperature image - derived from processings of NOAA - AVHRR data (southern India)

where, A is surface albedo; R_s is the incident short wave radiation (w/m^2); E_a is the atmospheric emissivity; R_l is the incoming long wave radiation (w/m^2); E_s is the surface emissivity; σ is the Stefan – Boltzman constant and T_s is the surface temperature ($^{\circ}K$).

Atmospheric emissivity (E_a) and incoming long wave radiation (R_l) can be computed using following expressions given by Brutsaert (1975) :

$$E_a = 1.24 (e_a / T_a)^{1/7}$$

$$R_L = \sigma \cdot T_a^4$$

where, e_a is the vapour pressure of air at ambient air temperature T_a . The sensible heat flux may be written as :

$$H = \rho \cdot C_p (T_s - T_a) / \gamma_a$$

where, ρ is the air density; C_p is the specific heat of air, γ_a is the aero-dynamic resistance for sensible heat flux (S/m). The aero-dynamic resistance (γ_a) can be expressed as (Hatfield *et al.*, 1984) :

$$\gamma_a = \frac{1_n \{(z-d)/z_0\}^2}{K^2 U}$$

where, Z is the reference height (2m); d is the zero plane of displacement (m) ($= 2 h/3$ h is the height of vegetation); Z_0 is the surface roughness height (m) ($= h/8$); K is the Von Karman's constant (≈ 0.38) and U is the wind speed at Z (m/s).

Soil heat flux can be written as function of net radiation (Ma *et al.*, 1999):

$$G = \frac{T_s (0.003.A + A^2) (1 - 0.978 \text{ NDVI } 4) \cdot R_n}{A} \quad (\text{for vegetated surface})$$

$$G = 0.20 \cdot R_n \quad (\text{for bare surface})$$

Since, H , G and R_n are instantaneous, it is necessary to apply a procedure to integrate to daily totals. The evaporative fraction (Brutsaert and Sugita, 1992) is the energy used for evaporation process divided by the total amount of energy available for the evaporation process.

$$\hat{=} = \frac{LH}{LH + H} = \frac{LE}{R_n - G}$$

Although, the H and LE fluctuate strongly on daily basis, the evaporative fraction behaves steady during day time. Then, the link between the instantaneous and the integrated daily case is given by

$$\hat{ET}_{24 \text{ hrs}} = \hat{ET}_{\text{inst.}}$$

The final equation that can be used to evaluate the daily ET is based on the evaporative fraction –

$$ET_{24} = \hat{ET}_{\text{inst.}} (R_n \text{ day} - G \text{ day})$$

Figure 6 illustrates flow chart for a daily ET model based on remote sensing data. Various researchers investigated several approaches of ET modeling using satellite data using Landsat TM and NOAA – AVHRR data (for reference see Chen *et al.*, 2003). ET and R_n estimated from Landsat TM data following surface energy balance modeling approach for western part of Doon Valley is presented in Fig. 7 (Saha and Pande, 1995b).

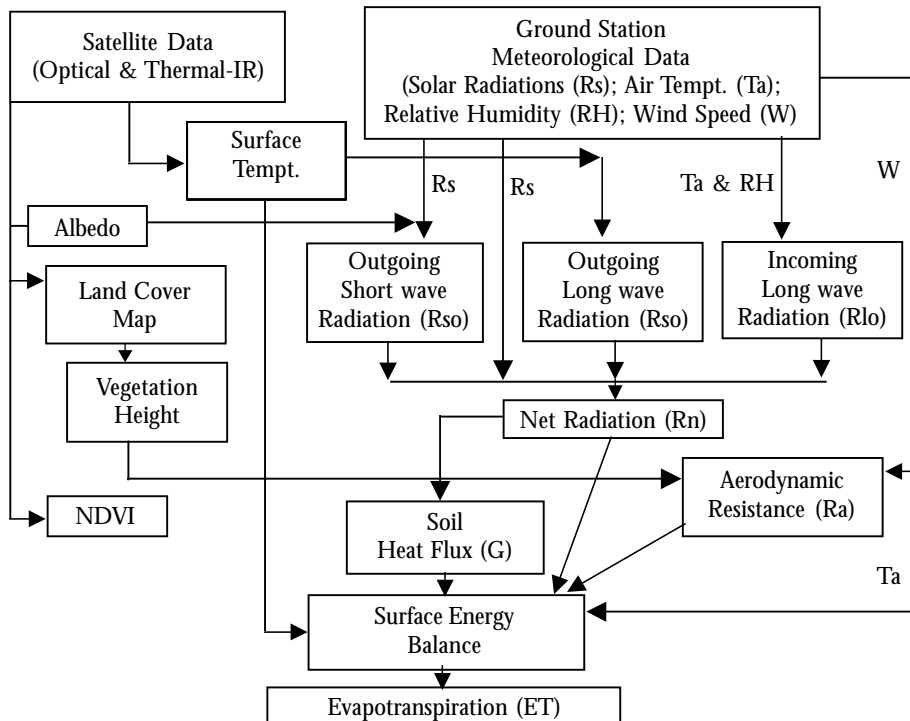


Figure 6: Flow chart for daily regional ET estimation using satellite data

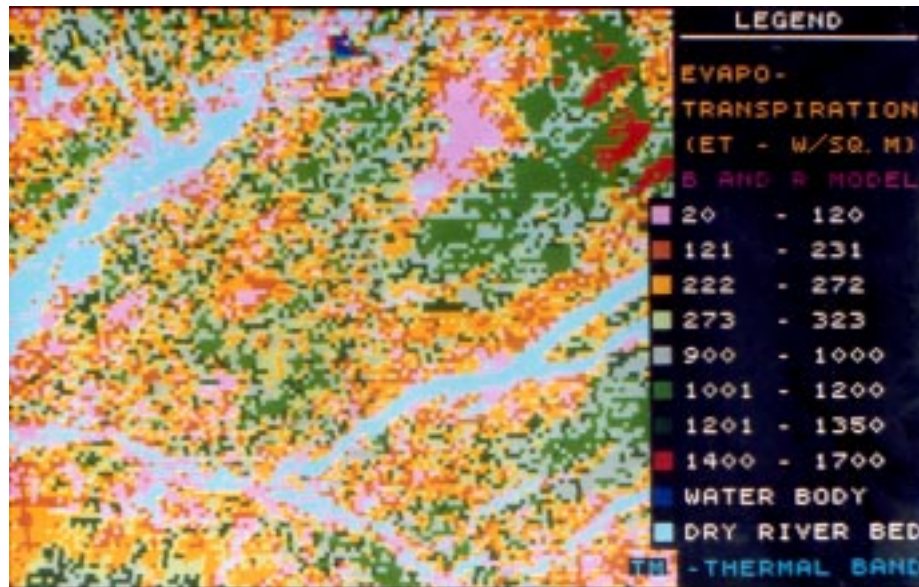


Figure 7: Evapotranspiration image of part of western Doon Valley generated by processing of Landsat – TM data

Absorbed Photosynthetically Active Radiation (APAR)

APAR is the fraction of the PAR (Photosynthetically Active Radiation) absorbed by the canopy and used for carbon dioxide assimilation. PAR refers to the visible part of the solar spectrum between 0.4 and 0.7 μm , where chlorophyll absorbs solar radiation. APAR is a key parameter in productivity analysis and ecosystem modeling. The productivity of vegetation canopies can be studied from estimation of APAR derived from optical remote sensing data.

The APAR results from a leaf radiation balance :

$$\text{APAR} = \text{PAR} - p_{\text{PAR}} \cdot \text{PAR} - \text{PAR}_{\text{trans}} + \text{PAR}_{\text{soil}}$$

where, p_{PAR} is the canopy reflectance at the upper side of the canopy in the 0.4 to 0.7 μm spectral range, $\text{PAR}_{\text{trans}}$ is the amount of PAR that is transmitted through the canopy and directed to the soil; PAR_{soil} that is reflected from the soil underneath the canopy and is received back at the lower side of the canopy.

APAR can be deduced directly from PAR after simplifying the previous equation into :

$$\text{APAR} = f\text{PAR} \cdot \text{PAR}$$

where, $f\text{PAR}$ is the fractional photosynthetically active radiation.

Asrar *et al.* (1992) showed that $f\text{PAR}$ is related to NDVI and relation is expressed by :

$$f\text{PAR} = 1.222 - 0.1914 \cdot \text{NDVI}$$

Variation in canopy optical properties, architecture as well as background spectral reflectance could affect $f\text{PAR}$ – NDVI relation, with background spectral properties producing a large effect.

It was observed that APAR was linearly related to NDVI and curvilinearly to LAI (Leaf Area Index) approaching asymptotically value of LAI, where virtually all incident short wave radiation observed by crop canopy. Fig. 8 illustrates APAR map of wheat crop derived by processing of IRS- WiFS data from a case study of part of U.P. and U.A., India (ASD, 2003).

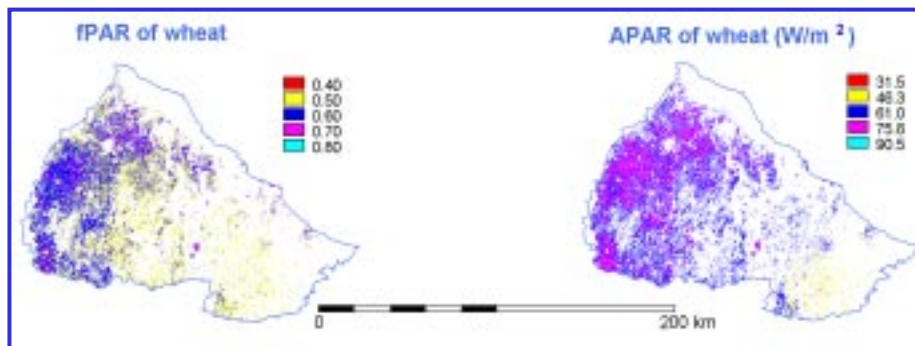


Figure 8: Estimated $f\text{PAR}$ and APAR values of wheat (using NDVI of IRS –WiFS).

Clevers (1989) suggested an approach for reducing soil background to some extent on the relation between $f\text{PAR}$ and remote sensing derived spectral indices. According to him $f\text{PAR}$ can be related with WDVI (Weighted Difference Vegetation Index).

$$f\text{PAR} = \text{WDVI} \cdot f\text{PAR}_\alpha / \text{WDVI}_\alpha$$

where, $f\text{PAR}_\alpha$ is asymptotically limiting value of $f\text{PAR}$ (usually 0.94); WDVI_α is the asymptotically limiting value of WDVI which is given by :

$$\text{WDVI} = \text{NIR}_t - C \cdot R_t$$

$$C = \frac{\text{NIR}_s}{R_s}$$

where, NIR_t is the total measured NIR reflectance, R_t is the total measured red reflectance, NIR_s and R_s are the NIR and red reflectance of soil, respectively.

The relation between LAI and f PAR was described as :

$$\text{LAI} = -1/K_{\text{PAR}} \cdot \ln [1 - f \text{ PAR} / f\text{PAR}\alpha]$$

where, K_{PAR} is the function of extinction and scattering co-efficient.

Experimental evidence indicated that the growth rate of several agricultural crop species increases linearly with increasing amounts of APAR, when soil water nutrients are not limiting (Myneni and Choudhury, 1993).

Therefore, integration of APAR over period e.g. growth cycle (i.e. emergence to maturity) represents total photosynthetic capacity of crops :

$$\text{APAR} = \int_{t=0}^m e \cdot \text{APAR}(t) = \int_{t=0}^m e \cdot f(\text{NDVI}) \cdot 0.48 \cdot R_s$$

where, e is the radiation use efficiency, defined as the ratio of canopy net photosynthesis to incident PAR; $f(\text{NDVI})$ is a function relating NDVI with f PAR and R_s is the incoming solar radiation. Field *et al.* (1995) developed a global ecology model for net primary production in which e is calculated as :

$$e = e' \cdot T_1 \cdot T_2 \cdot W$$

where, e' is the typical maximum conversion factor for above ground biomass for C_3 and C_4 crops when the environmental conditions are all optimum ($e = 2.5$ for C_3 crops and $e = 4$ for C_4 crops).

$$W = \wedge$$

$$T_1 = 0.8 + 0.02 \cdot T_{\text{opt}} - 0.005 \cdot T_{\text{opt}}^2$$

$$T_2 = 1.185 \frac{1}{1 + \exp(0.2 \cdot T_{\text{opt}} - 10 - T_{\text{mon}})} \cdot \frac{1}{1 + \exp(-0.3 T_{\text{opt}}^{-10} + T_{\text{mon}})}$$

where, \wedge is the evaporative fraction, T_{opt} ($^{\circ}\text{C}$) is the mean air temperature during the month of maximum LAI or NDVI and T_{mon} ($^{\circ}\text{C}$) is the mean monthly air temperature.

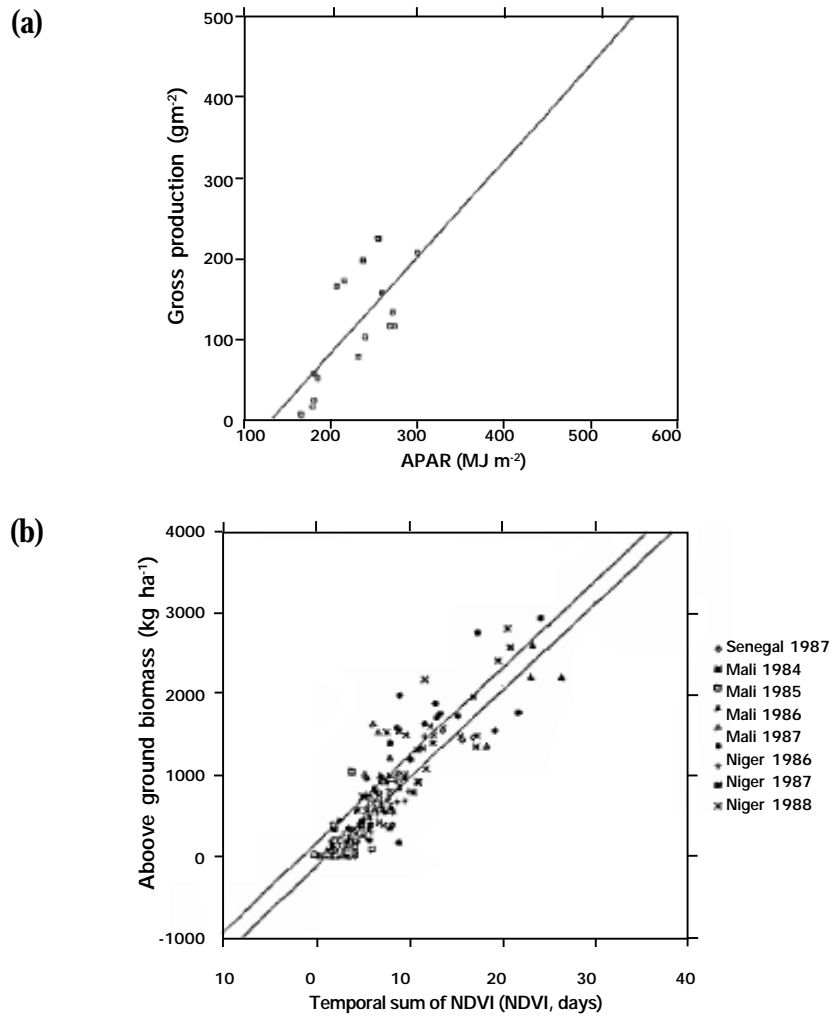


Figure 9: (a) Relation between gross production and accumulated APAR and (b) Relation between above ground biomass and accumulated NDVI

Therefore, temporal sums of NDVI which is giving cumulative values of APAR, can be used for estimation of crop/vegetation productivity. Prince (1990) observed a good linear relationship between APAR and vegetation gross production and also strong positive relationship between above ground vegetation biomass and temporal sum of NOAA – AVHRR NDVI (Fig. 9) in parts of Africa.

CONCLUSIONS

Remotely sensed satellite optical and thermal infrared can be synergistically used to estimate surface agro-meteorological properties. Optical data can be used to estimate land surface albedo by integrating narrow-band directional spectral reflectances. Thermal IR data from various satellites appear as valuable tool for vegetation growth and conditions assessment by retrieval of land surface temperature and estimation of evapotranspiration following various modeling approaches. Optical data in the form of spectral indices are found to be related to solar radiation absorbed by vegetation canopies and this is useful for assessing regional vegetation potential productivity.

REFERENCES

- Asrar, G. Myneni, R.B. and Choudhury, B.J. 1992. Spatial heterogeneity in vegetation canopies and remote sensing of absorbed photosynthetically active radiation : a modeling study. *Remote Sensing Environment*, 41 : 85-103.
- Bartholic, J. F., Namken, K.N. and Wiegand, C.L. 1972. Aerial thermal scanner to determine temperature of soil and crop canopies differing in water stress. *Agronomy Journal*, 6 : 603.
- Becker, F. and Li, L. 1990. Towards a local split window method over land surface. *Remote Sensing Environment*, 32 (17) : 17-33.
- Brest, C.L. and Goward, S.N. 1987. Deriving surface albedo from narrow band satellite data. *International Journal of Remote Sensing*, 8 : 351-367.
- Brown, K.W. 1974. Calculation of evapotranspiration from crop surface temperature. *Agricultural Meteorology*, 14 : 199-209.
- Brutsaert, W. 1975. On a derivable formula of long wave radiation from clear skies. *Water Resource Research*, 11 : 742 – 744.

- Brutsaert, W. and Sugita 1992. Application of self-preservation in the diurnal evolution of the surface energy budget to determine daily evaporation. *Journal of Geophysical Research*, 19 (17) : 18, 377 – 18, 382.
- Chen, Y.; Li, X.; Jing, G. and Shi, P. 2003. An estimation model for daily regional evapotranspiration. *International Journal of Remote Sensing*, 24 : 199 – 205.
- Clevers, J.G.P.W. 1988. A simplified reflectance model for the estimation of Leaf Area Index. *Remote Sensing Environment*, 25 : 53-69.
- Field, C.B.; Randerson, J.J. and Malmstrom, C.M. 1995. Global net primary productivity production : Combining ecology and remote sensing. *Remote Sensing Environment*, 51 (1) : 74-88.
- Goita, K. and Royer, A. 1992. Land surface climatology and land cover change monitoring since 1973 over a north-Sahelian zone using Landsat data. *Geocarto-International*, 2: 15-28.
- Hatfield, J.L.; Reginato, R.J. and Idso, S.B. 1984. Evaluation of canopy temperature evapotranspiration models over various crops. *Agricultural and Forest Meteorology*, 32: 41 – 53.
- Kant, Yogesh 2000. Studies on Land Surface Process using Satellite Data. *Ph.D. Thesis* in Physics, Omania University, India.
- Myneni, R.B. and Choudhary, B.J. 1993. Synergistic use of Optical and Microwave data in agro-meteorological applications. *Advances in Space Research*, 13 (5) : 239-248.
- Mansor, S.B. and Cracknell, A.P. 1994. Monitoring of coal fires using thermal infrared data. *International Journal of Remote Sensing*, 15 (8) : 1675 – 1685.
- Prasad, S.; Gupta, R.K. and Sesa Sai, M.V.R. 1995. Computation of surface albedo from NOAA – AVHRR data. Pages 51-57. In Proc. National Symposium on Remote Sensing Environment with special emphasis on Green Revolution. ISRS, India.
- Prince, S.D. 1990. High temporal frequency remote sensing of primary production using NOAA – AVHRR. Pages 169-184. In book “Applications of Remote Sensing in Agriculture” (Eds. M.D. Steven and J.A. Clark). Butterworth.
- Saha, S.K. and Pande, L.M.1995a. Regional surface albedo and ET modeling using combination of optical and thermal IR data. Pages 70-78. In book “Advances in Tropical Meteorology” (R.K. Dutta, Ed.). Concept Publishers, New Delhi, India.
- Saha, S.K. and Pande, L.M.1995b. Modeling land surface energy balance components and assessment of crop water stress – a satellite thermal IR remote sensing approach. Proc. ISRS Silver Jubilee Year Seminar, Dehra Dun.

- Saunders, R.W. 1990. In determination of broad band surface albedo from AVHRR visible and near infrared radiances. *International Journal of Remote Sensing*, 11 (1) : 49 – 67.
- Valor, E. and Caselles, V. 1996. Mapping land surface emissivity from NDVI; application to European, Africa and South American areas. *Remote Sensing Environment*, 57 : 167 – 184.
- van de Gried, A.A. and Owe, M.1993. On the relationship between thermal emissivity and the normalized difference vegetation index for natural surfaces. *International Journal of Remote Sensing*, 14 : 1119 – 1131.
- Valientz, J.A.; Nunez, M.; Lopez – Baeza E. and Poreno, J.F. 1995. Narrow band to broad band conversion for Meteosat – visible channel and broad – band albedo using both AVHRR –1 and 2 channels. *International Journal of Remote Sensing*, 16 (6) : 1147 – 1166.